

Earth and Space Science



RESEARCH ARTICLE

10.1029/2024EA004167

Key Points:

- A machine learning model was developed to predict low-latitude vertical plasma drift from total electron content data
- The VIPER model is based on a multi-layer perceptron architecture and has uncertainty quantification built-in
- Test results demonstrate that VIPER can capture day-to-day vertical plasma drift on a global scale

Correspondence to:

X. Pi,
xiaoqing.pi@jpl.nasa.gov

Citation:

Reddy, S. A., Pi, X., Forsyth, C., Aruliah, A., & Smith, A. (2025). Predictions of equatorial vertical plasma drift using TEC data and a neural network model. *Earth and Space Science*, 12, e2024EA004167. <https://doi.org/10.1029/2024EA004167>






Received 4 FEB 2025
Accepted 23 MAY 2025

Author Contributions:

Conceptualization: X. Pi
Data curation: S. A. Reddy, X. Pi
Formal analysis: S. A. Reddy, X. Pi
Investigation: S. A. Reddy, X. Pi, C. Forsyth, A. Aruliah, A. Smith
Methodology: S. A. Reddy, X. Pi, C. Forsyth, A. Aruliah, A. Smith
Project administration: X. Pi
Resources: X. Pi
Software: S. A. Reddy, A. Smith
Supervision: X. Pi
Validation: S. A. Reddy, X. Pi
Visualization: S. A. Reddy
Writing – original draft: S. A. Reddy
Writing – review & editing: X. Pi, C. Forsyth, A. Aruliah, A. Smith

© 2025. Jet Propulsion Laboratory, California Institute of Technology. Government sponsorship acknowledged. Earth and Space Science published by Wiley Periodicals LLC on behalf of American Geophysical Union. This is an open access article under the terms of the [Creative Commons Attribution-NonCommercial License](#), which permits use, distribution and reproduction in any medium, provided the original work is properly cited and is not used for commercial purposes.

Predictions of Equatorial Vertical Plasma Drift Using TEC Data and a Neural Network Model

S. A. Reddy^{1,2} , X. Pi¹ , C. Forsyth² , A. Aruliah³ , and A. Smith⁴ 

¹Jet Propulsion Laboratory, California Institute of Technology, Pasadena, CA, USA, ²Mullard Space Science Laboratory, University College London, Dorking, UK, ³Department of Physics and Astronomy, University College London, London, UK, ⁴Department of Mathematics, Physics and Electrical Engineering, Northumbria University, Newcastle upon Tyne, UK

Abstract Vertical plasma drift, v_z , plays a key role in the dynamics, morphology, and space weather effects of the equatorial and low latitude ionosphere. Modeling the drift has been an on-going effort for climatology-based prediction. To address daily prediction, the *Vertical drifts: Predicting Equatorial ionospheric dynamics* (VIPER) model has been developed. VIPER is a machine learning model that is trained on total electron content (TEC) data to predict low-latitude vertical plasma drift observed by the C/NOFS mission across the period 2009–2015. The uniqueness of VIPER is that it uses TEC data for the prediction, and the data is globally and readily available. A Gaussian fitting routine is developed to strengthen the link between TEC and v_z . VIPER is a multi-layer perceptron framework with Monte Carlo (MC) uncertainty estimation capabilities. It has a mean absolute error of 8.3 m/s, an R of 0.89/1, and a skill of 0.78/1, all of which are strong scores. The model is capped at quiet and unsettled activity levels ($K_p < 3$). MC analysis reveals that predictions should be interpreted as distributions and the uncertainty can vary with distributions of TEC data and regions of prediction even if the predicted value is the same. VIPER offers longitudinally global coverage and uncertainty estimation capabilities. It could also be expanded to handle storm-time conditions with additional work.

Plain Language Summary The motion of plasma is responsible for transporting particles and energy from one region of Earth's ionosphere to another, changing its state, characteristics, and behavior. Over the years, studies have aimed to predict this plasma motion (drift), but most have focused on climatological patterns rather than daily or weather variations. To address this, the *Vertical drifts: Predicting Equatorial ionospheric dynamics* (VIPER) model has been developed. VIPER is a machine learning model that is trained on total electron content (TEC) data to predict the vertical plasma drift observed by the C/NOFS mission from 2009 to 2015. The uniqueness of VIPER is that it uses TEC data for the prediction, and the data is readily available. VIPER offers global coverage and uncertainty estimation capabilities. The next step for VIPER is to make predictions during geomagnetic storms.

1. Introduction

Vertical plasma drift, v_z , plays a key role in the equatorial and low-latitude ionosphere, modifying its electron density distribution mostly in latitude and altitude dimensions. At the magnetic equator, vertical plasma drift is also known as the $\mathbf{E} \times \mathbf{B}$ drift, a direct consequence of the Lorentz force and its constituent zonal electric and ambient geomagnetic fields. The $\mathbf{E} \times \mathbf{B}$ drift can push ionospheric plasma to different altitudes where the plasma lifetime is longer or shorter depending on the ion and electron recombination and molecular dissociation rates in the region. At latitudes off the magnetic equator, in addition to the $\mathbf{E} \times \mathbf{B}$ drift, the neutral wind also exerts a significant influence on the dynamics and distribution of plasma. In the low-latitude F region, the wind can push plasma to move along the magnetic field lines, bringing it to higher or lower altitudes. During quiet times, v_z magnitudes are generally between -40 and 40 m/s (e.g., Fejer et al., 2008; Immel et al., 2021; Scherliess & Fejer, 1999). These dynamical effects modulate the peak electron densities and its altitude. The $\mathbf{E} \times \mathbf{B}$ drift and wind are crucial inputs to physics-based uncoupled global ionospheric models.

One of the characteristics of ionospheric variations at low latitudes due to the dynamical effects is the Equatorial Ionization Anomaly (EIA) phenomenon (Appleton, 1946). It features two plasma density or total electron content (TEC) crests around $\pm 15^\circ$ magnetic latitude (Mlat) and an ionization trough at the magnetic equator. The EIA is attributed to the *equatorial fountain effect* (e.g., Martyn, 1955; Mitra, 1946), that is, as the plasma is pushed to higher altitudes, it diffuses poleward along the magnetic field lines under the action of gravity and pressure

gradients. The EIA crests are easily identifiable in latitudinal profile of total electron content (TEC), and in Global Ionospheric Maps (GIMs) (e.g., Iijima et al., 1999; Mannucci et al., 1998) as well as in global assimilative models (e.g., Pi et al., 2009).

Several previous studies have successfully predicted different aspects of vertical plasma drift. Scherliess and Fejer (1999) developed an empirical model for predicting v_z using the ion drift meter observations on the Atmospheric Explore E (AE-E) spacecraft. Their climatological model operates during quiet-times ($K_p < 3$) and is based on earlier observations using the same spacecraft, which discussed the effects of solar activity, season, and longitude on v_z (Fejer et al., 1995). Anderson et al. (2004) built a neural network using ground-based geomagnetic measurements to predict daytime vertical $\mathbf{E} \times \mathbf{B}$ drift between 10 and 16 LT. More recently, Shidler and Rodrigues (2020) predicted quiet-time localized vertical plasma drift using Jicamarca observatory data and a random forest regressor. They used UT, day-of-the-year, solar flux and altitude as inputs, and they compared their results with the Scherliess and Fejer (1999) model. Later based on ROCSAT-1 data, Fejer et al. (2008) developed an empirical equatorial F region vertical drift model for geomagnetically quiet conditions; this was followed up by Kil et al. (2009) who developed a high-longitude-resolution model using data from the same spacecraft. Both studies validate their findings against the Jicamarca radar data.

In this study we present *Vertical drIFts: Predicting EquatoRIal dynamics* (VIPER). VIPER is a machine learning model that predicts vertical plasma drift (v_z) in the equatorial and low latitude ionosphere using TEC data, whilst also estimating the uncertainty of its predictions. VIPER is the first-of-its-kind and could be used as a test bed for future research into daily (weather) v_z predictions. First, we describe the data sets, followed by the novel Gaussian fitting routine to extract meaningful quantities from the TEC data. Then we perform feature engineering, creating new features before presenting the ML architecture and optimized parameters. Finally, we showcase the results and discuss the performance with respect to the existing models and frameworks.

2. Data and Instrumentation

TEC is the column density measured in electrons per square meter, that is, the integral of ionospheric electron density distributed along a specific direction. It is usually measured in TEC units ($1 \text{ TECU} = 10^{16} \text{ electrons/m}^2$). Such line-of-sight TEC can also be converted to vertical direction, and the process of slant to vertical mapping is well established (e.g., Iijima et al., 1999; Mannucci et al., 1998). GIMs are TEC products whereby all the TEC values are projected onto a single map at a specific time interval. This study utilizes the publicly available Jet Propulsion Laboratory (JPL) GIM database (https://sideshow.jpl.nasa.gov/pub/iono_daily/gim_for_research/jpld/). The GIMs are generated every 15 min from 200 ground stations. An example GIM captured at 0130 LT on the 21 December 2014 is shown in Figure 1. The EIA is observable in the Pacific region as a ~ 115 TECU enhancement at $\pm 15^\circ$ latitude. Also shown are the ground stations (white dots) and the day-night terminator at 0 km.

We convert the JPL GIMs into magnetic coordinates using the *ApexPy* package (<https://pypi.org/project/apexpy/>). *ApexPy* is a Python wrapper based on the original Apex Fortran code (Emmert et al., 2010; Meeren et al., 2021). It takes geographic latitude, longitude, altitude as inputs and outputs magnetic latitude and magnetic local time using the process developed by Richmond (1995). We then average over all 96 daily GIMs sampled at 15 min, to produce a single 24 hr map for each date. This is necessary to pair the 2D GIMs with the 1D satellite measurements of v_z . In addition, we split geographic longitude into eight sectors across -180° – 180° using the same boundaries as Fejer et al. (2008).

We use v_z data from the Ion Velocity Meter (IVM) onboard the Communications/Navigation Outage Forecasting System (C/NOFS) satellite across the period January 2009 to August 2015. The v_z data covers all vertical drift between -28° and 28° Mlat, including vertical $\mathbf{E} \times \mathbf{B}$ drift at the equator. We chose to predict vertical drift for two main reasons: it is the original data provided by the IVM, and TEC at low latitudes ($\pm 28^\circ$ Mlat) is largely determined by multi-dynamical effects, including not only vertical $\mathbf{E} \times \mathbf{B}$ drift, but also wind-driven drift and diffusion effects. The IVM data covers the ascending phase of solar cycle 24. Solar minimum during this period was particularly deep with < 10 sunspot numbers for most of 2009. C/NOFS had a low inclination orbit of 13° and a moderately elliptical orbit of 375 km (perigee) and 850 km (apogee) (De La Beaujardière, 2004). A limitation of the IVM is that data should only be used when $N_i(\text{O}^+) > 8 \times 10^3 \text{ cm}^{-3}$ (correspondence with R. Heelis, IVM Principal Investigator). This means there is less data available during post-midnight hours (00–06 MLT) when the electron density is naturally lower owing to continuous chemical recombination and a lack of substantial ion

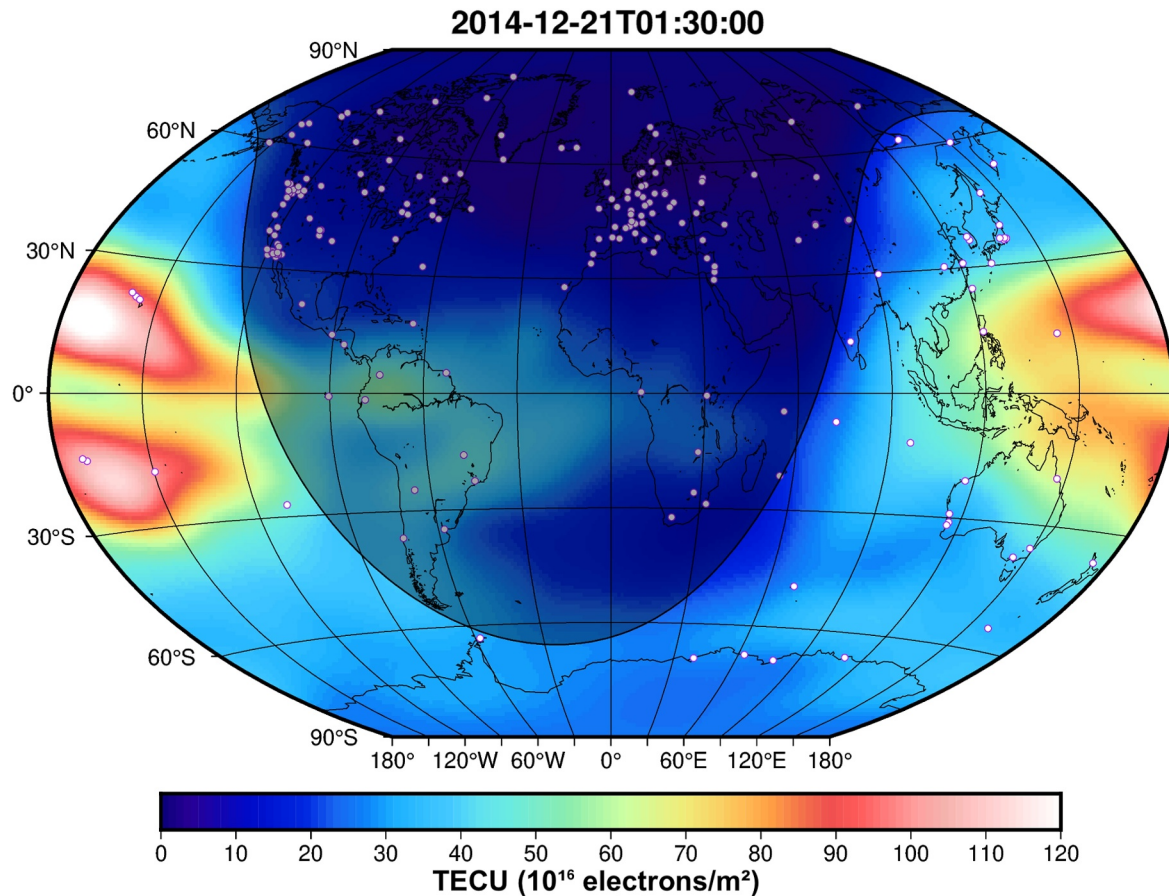


Figure 1. An example GIM on 2014-12-21 at 0130 UTC. The EIA is observed in the Pacific region. The white dots represent the ground stations and the day-night terminator at 0 km highlights the dependence of TEC on solar insolation.

photoionization, which is more eminent during low solar activity than high solar activity years. This adds an unavoidable imbalance in the data set across local time and solar activity.

We remove any data where $K_p > 3$, which means that VIPER is a quiet ($K_p = 0-2$) and somewhat unsettled ($K_p = 2-3$), time model only. This decision was primarily based on the limited amount of drift data during space weather and geomagnetic active conditions. Future works may include $K_p > 3$ data and this is considered further in the Discussion section. We only use IVM data which has a flag of 0 which indicates it is of the highest quality. Finally, the IVM data is converted from a time series and binned by date, Mlat, MLT, and Glon which provides a like-for-like with the GIM data. At this stage the vertical drift values from C/NOFS are directly mapped to corresponding TEC values.

3. Feature Engineering

To improve the prediction power of VIPER, we develop a novel fitting routine to strengthen the association between TEC and v_z . This process is informed by the characteristics of vertical drift, its relationship with the EIA, and the influence of the model inputs, such as local time or the SYM-H index.

3.1. Fitting Routine

The EIA is driven by vertical plasma drift, which is a combination of $\mathbf{E} \times \mathbf{B}$ drift, wind, gravitational effects, and pressure gradients. To identify and quantify the features of the EIA, we fit two independent Gaussians to the TEC data: one for the northern hemisphere and one for southern. The fit is performed using the Levenberg-Marquardt (LM) algorithm (Moré, 1978), and the LM fit module for Python (<https://lmfit.github.io/lmfit-py/>). We modify a traditional Gaussian expression to also include a “peak magnitude” parameter α ,

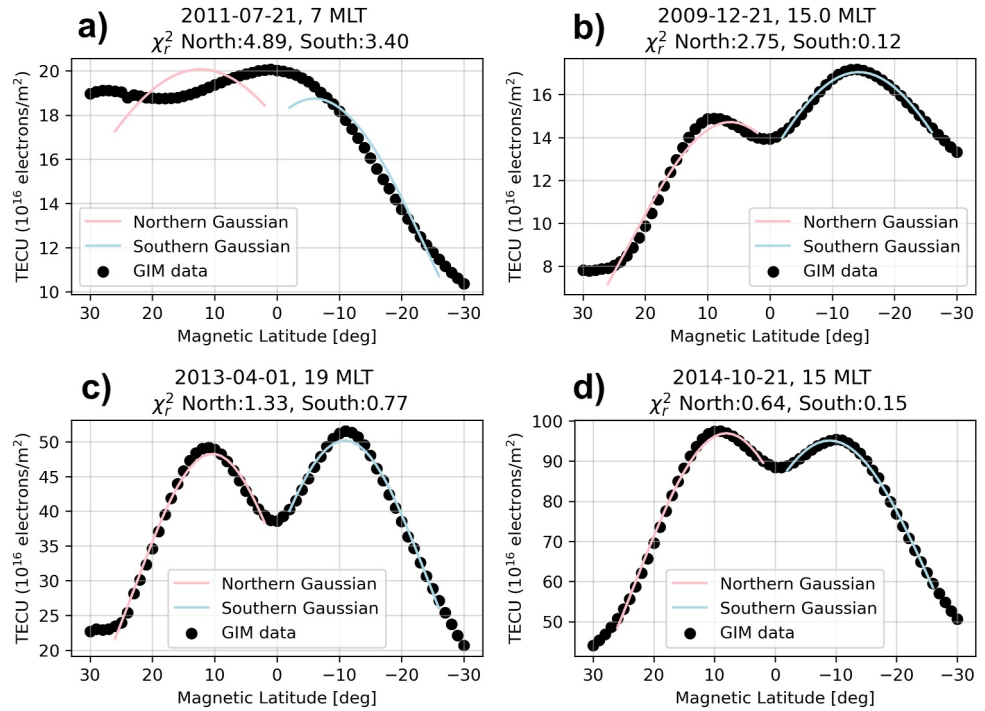


Figure 2. Gaussian fitting routine applied to four example TEC distributions. The fitting routine has the best fit and lowest χ_r^2 in the bottom panel (c–d) and the worst fits in the top (a–b). The dates and local times indicate that the fit is best during the day or immediately post-sunset and during the equinoxes. This is when the EIA is most likely to occur and is most symmetric.

$$f(t, \phi, \lambda) = \alpha \cdot \exp\left(-\frac{(\lambda - \mu)^2}{2 \cdot \sigma}\right) \quad (1)$$

where f represents the TEC values for a given magnetic local time t and geographic longitude ϕ , across all concerned magnetic low latitudes λ . α is the value of the peak of the Gaussian in TECU, μ is location of the peak in Mlat, and σ is the latitudinal width of the distribution. We assess the quality of the Gaussian fit using the *reduced chi squared* χ_r^2 score

$$\chi_r^2 = \sum_i^N r_i^2 / (N - N_v) \quad (2)$$

where r_i is the residual error after the least-squares LM optimization, N is the number of data samples, and N_v is the number of parameters. As χ_r^2 is largely driven by the residuals, r_i , a smaller value indicates a better fit. To constrain the fit and improve processing times, we place upper and lower bounds on the parameters to be optimized: $\alpha = 60$ to 150 TECU; $\mu = 7^\circ$ to 20° Mlat; and $\sigma \leq 19^\circ$ Mlat.

Figure 2 shows a selection of fits across different seasons and local times. In Figure 2a we do not observe any EIA and this is correctly reflected by the poor fit of the *Northern Gaussian* and *Southern Gaussian* to the data, and the high χ_r^2 scores. In Figure 2b, we see that the fits are improved, but mainly in the southern hemisphere, indicating an asymmetric EIA. In the bottom panels, we see good quality fits as indicated by $\chi_r^2 < 1.5$ (Figures 2c and 2d). This suggests that the distributions are close to the symmetric EIA. To identify when the EIA is present, we rely on a low χ_r^2 and reject any fits where $\chi_r^2 > 2$. We also mandate that the EIA cannot occur close to the equator (Mlat $> 7^\circ$) and that the width of the peaks must not exceed $\pm 20^\circ$ Mlat. This is because the data is only examined over $\sim 30^\circ$ in each hemisphere.

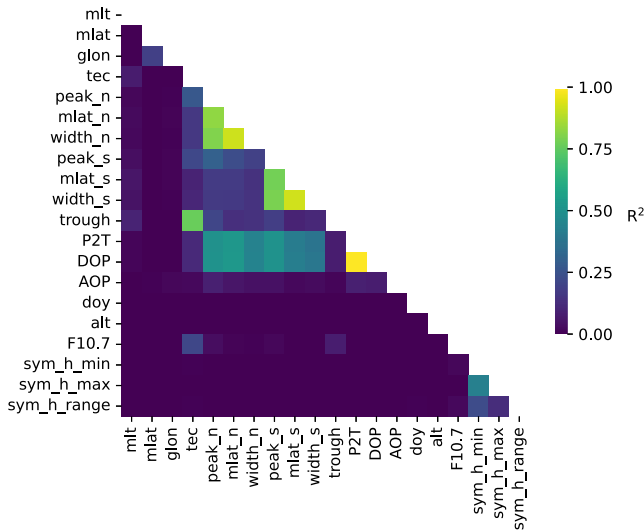


Figure 3. The model inputs and their linear relationships (see Equation 9).

3.2. EIA Features

Once we have established that a distribution of TEC is likely to be the EIA, we then define another set of variables from the data. Firstly, the Peak-2-Trough (P2T) magnitude,

$$P2T = \frac{((\alpha_n + \alpha_s) / 2)}{\text{trough}}, \quad (3)$$

where α_n and α_s represent the peak TECU values for the northern and southern hemispheres, respectively, and *trough* is the TECU value at 0° Mlat. Next, Distance Of the Peaks (DOP), which may also relate to the magnitude of v_z at and near the magnetic equator,

$$DOP = |\mu_n - \mu_s|. \quad (4)$$

Finally, Asymmetry Of the Peaks (AOP), which assesses the asymmetry between the northern and southern hemispheres. Quantifying the asymmetry is important because it can be caused by the inter-hemispheric wind and hemispheric asymmetries in ion production during non-equinox months,

$$AOP = \frac{(\alpha_n - \alpha_s)}{(\alpha_n + \alpha_s)} * 100. \quad (5)$$

The purpose of these additional features is to further help the model connect v_z magnitudes with the characteristics of the EIA. For example, if the P2T is large, DOP is roughly 30°, and the AOP is close to 0, then the EIA is likely dominated by the upward $\mathbf{E} \times \mathbf{B}$ drift. The model can capture vertical $\mathbf{E} \times \mathbf{B}$ drift when Mlat \approx 0°. Finally, we must also deal with cyclical features, such as day-of-the-year, longitude, and MLT. We convert these values into signals with

$$\sin \frac{2\pi\gamma}{n}, \cos \frac{2\pi\gamma}{n}, \quad (6)$$

where γ is the feature to be turned into a signal and n is the maximum frequency of that signal. For example, $n = 365$ for day-of-the-year, $n = 360^\circ$ for longitude, or $n = 24$ for MLT. The process described above is outlined in Figure A1 of Appendix A.

3.3. Feature Inputs

Figure 3 shows the model inputs and the R^2 relationship between them. Generally, there is little-to-no correlation between the features. In some instances, linear correlation is expected. For example, we expect the width of the peaks to increase with their location in magnetic latitude. Despite these relationships, it is helpful to keep certain correlated features for post-training analysis in order to link the predictions back to the physics of the system.

For our input selection, we considered the works of Anderson et al. (2004), Fejer et al. (1995), and Shidler and Rodrigues (2020), and the availability of the data. For example, we exclude any inputs which are not readily available data products or rely on other models (e.g., wind or chemical constituents). As we are predicting on a daily basis, SYM-H has been represented by its daily minimum, maximum, and range. The total numbers of samples are ~930 k, with 744 k for training, 93 k for testing, and 93 k for validation (80%–10%–10% split).

4. Machine Learning

To predict v_z from TEC, we use a machine learning approach. Specifically, we use a Multi-Layer Perceptron (MLP) model, which is a fully connected feed-forward neural network (Popescu et al., 2009)

Table 1
Hyper-Parameter Optimization for VIPER

Hyperparameter	Search range	VIPER
N_e in layer 1	64–1,024	1,024
N_e in layer 2	64–1,024	512
N_e in layer 3	32–512	256
N_e in layer 4	32–512	128
Dropout Rate	0.05–0.3	0.2
Learning Rate	10^{-5} – 10^{-2}	10^{-3}
Batch Size	8–256	128

Note. We tested several combinations and the final selection offers a good balance of performance, generalization, and training time.

$$\hat{y}(x) \approx \sum_{i=1}^{N(e)} a_i \sigma(w_i \cdot x + b_i), \quad (7)$$

where:

- \hat{y} is the VIPER prediction of v_z
- N_e is the number of neurons in the hidden layers, which is optimized and finalized in Table 1
- a_i is the weight associated with the i -th neuron in the output layer
- σ is the ReLU activation function
- w_i is the weight vector associated with the i -th neuron in the hidden layer
- x is the feature input vector to the MLP (see Figure 3)
- b_i is the bias term associated with the i -th neuron in the hidden layer

During the training process, the model computes the difference between the predicted v_z and the actual v_z from C/NOFS drift data. This error (see Equation 8) is then used to adjust the model's weights and biases through backpropagation, ensuring that the model learns from both TEC and drift data. Table 1 shows the number of layers and neurons N_e in the MLP, the neuron search range, and final choice of values. Training and optimization were performed on a high-performance computing cluster hosted at the UCL Mullard Space Science Laboratory. The setup consisted of a 128×64 -core processors at 2.0 GHz and $1 \times$ NVIDIA A-100 GPU with 40 GB of RAM. The training and optimization time was between 2 and 15 min. The final hyperparameter selection was based on performance (lowest possible error in m/s), as well as generalization (acceptable overfitting), and training time (<15 min on the MSSL GPU).

Lastly, we also used a step function to anneal the learning rate, reducing it by a factor of 0.6 every 10 epochs. This further improves model convergence and reduces the training time.

4.1. Assessment Metrics

Several metrics are used to assess the performance, association (R), and skill of the VIPER model. *Mean Absolute Error* (MAE) is a typical performance test for regression problems (Chai & Draxler, 2014),

$$\text{MAE} = \frac{1}{n} \sum_{i=1}^n |(\hat{y}_i - y_i)| \quad (8)$$

where y_i is the C/NOFS IVM measurement of v_z (target variable), \hat{y}_i is the prediction of y_i , and n is the number of samples. Accuracy metrics tell us how close the prediction is to the true value, but they do not tell us how well the model captures the up-and-down trends of the data set. Further, errors scale with the range of the target variable, and vertical drift is known to vary across local time, geolocation, season and geomagnetic activity. To combat this, we also use the Pearson correlation coefficient R

$$R = \frac{\sum (y_i - \bar{y})(\hat{y}_i - \bar{\hat{y}})}{\sqrt{\sum (y_i - \bar{y})^2 \sum (\hat{y}_i - \bar{\hat{y}})^2}}. \quad (9)$$

This tells us if the predictions are close to the target in some part of the data range, but not in others. An ideal value is $R = 1$. Finally, we examine the skill of the model by looking at its *Prediction Efficiency* which is based on its mean square error (Murphy, 1988)

$$\text{PE} = 1 - \frac{\sum (\hat{y}_i - y_i)^2}{\sum (y_i - \bar{y})^2}. \quad (10)$$

A model with perfect skill has a $\text{PE} = 1$, while $\text{PE} < 0$ shows that the model is no better at making predictions than the average of the target values, $\langle y \rangle$.

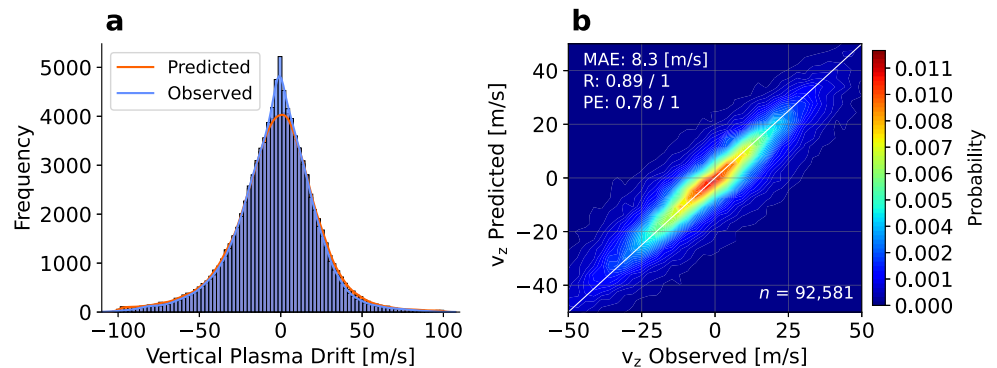


Figure 4. VIPER performance on the 10% test set, whose size is ~ 93 k samples. (a) VIPER predicts both upward and downward drift well, with limited levels of under- or over-estimation. (b) The probability of prediction-observation pairs and model performance. VIPER has a MAE of 8.3 m/s, R of 0.89, and skill of 0.78.

5. Results

The following section outlines the prediction capability of the VIPER model. Its performance is assessed for low latitudes globally (longitudinal wise) and then across its features. We then introduce the Monte Carlo dropout technique and estimates of prediction uncertainty, before presenting a preliminary examination of daily predictions.

5.1. Performance and Errors

Firstly, we examine the performance against the test set whose size is $n \approx 93$ k samples. Figure 4a shows VIPER performance in terms of the frequency of predictions versus observations. It also shows that although the *observed* distribution is Gaussian-like, there are more negative vertical drifts than positive ones. This is supported by the mean vertical drift value, which is -3 m/s.

The model underestimates the frequency of 0 m/s drift and overestimates those from $\geq +20$ m/s. Further imbalances between the upward and downward drift were also caused by the removal of lower quality data during the ML preparation process. This suggests that upward drifts have more flags, and potentially more errors, and this cannot be avoided at this stage. Figure 4b is a 2D histogram that shows the probability of various prediction and observation pairs. A perfect model, with an error of 0 m/s, would place the entire distribution on the white diagonal line. VIPER performs well, with the probability distributions in-line with those shown in Figure 4a. The model has a MAE error of 8.3 m/s, an R score of 0.89/1, and a PE of 0.79/1, all of which are strong scores. A R of 0.5–0.7 is said to be good in magnetospheric modeling applications (Liemohn et al., 2021), although this is only a general rule-of-thumb.

Figure 4 tells us how the model is performing at a global level, but it does not tell us how well it is doing across the various inputs. For example, does VIPER perform better at specific times or locations? Figure 5 shows the error, $\hat{y} - y$, across the feature space. Error bars are calculated using the standard error.

Generally, the error tracks to the availability of the data (gray histograms). Performance is consistent across most features but shows the greatest variance in magnetic local time. For example, the error doubles when making a prediction at 6 MLT compared to 15 MLT (Figure 5a).

Figure 6 examines the derived EIA data products (Equations 3–5) as a function of VIPER error, also using the standard error. Firstly, we see VIPER performs well across a range of DOP's, but the error increases when the data diminishes around 28° Mlat. DOP can be a proxy for an EIA effect of geomagnetic activity, which can be enhanced under active magnetic conditions. Secondly, VIPER performs best when the peak asymmetry is between -5 and 5 (Figure 6b), which is most common around the equinoxes (e.g., Balan et al., 2013, 2018). AOP is also associated with trans-hemispheric winds (e.g., Hanson & Moffett, 1966; Huang et al., 2018), but VIPER does not have the ability to confirm if this is the primary driver. Finally, when the Peak-2-Trough (P2T) ratio is lower, so too is the error (Figure 6c). A low P2T means that the EIA is less prominent or absent, which in turn indicates that vertical $\mathbf{E} \times \mathbf{B}$ drift magnitudes are small. This corresponds to a VIPER prediction of $v_z \approx 0$ m/s near the equator.

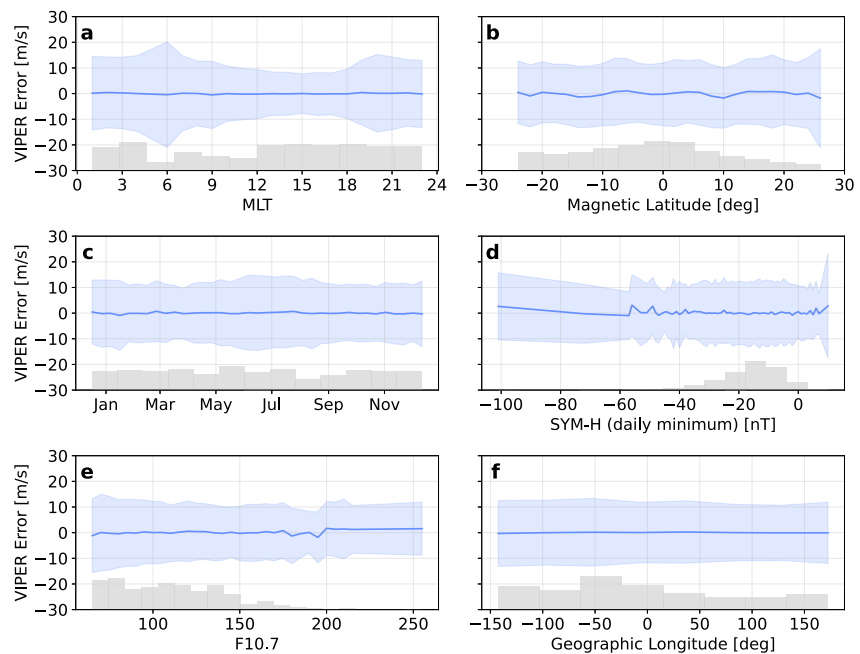


Figure 5. VIPER errors across six selected features within the test set. 0 m/s is a perfect score. The uncertainties are calculated via a bootstrapping method, and are represented by the shaded areas. The gray histogram bars represent the availability of the data.

5.2. Monte Carlo Uncertainty

To better understand the uncertainty within VIPER, we adopt the *Monte Carlo drop out* technique developed by Gal and Ghahramani (2016). *Dropout* is a type of *regularization* to prevent overfitting and it involves randomly removing neurons during the training process (Srivastava et al., 2014).

Like regular dropout, neurons are randomly deactivated, but with MC Dropout this occurs during both training and when making a prediction (evaluation). This means that each prediction of plasma drift will differ for a single set of inputs. By making multiple predictions from a single set of features, a probability distribution function emerges thus giving us the uncertainty of a prediction. MC dropout is a Gaussian-approximate method, but without a prohibitive computation cost (Gal & Ghahramani, 2016).

Figure 7 shows the Monte Carlo uncertainty of four example v_z predictions in the test set. The distribution consists of 500 MC samples, which is considered high enough to enable good statistics, without being computationally expensive. As seen, the distributions are non-Gaussian and the use of mean or standard deviation is not appropriate (Figure 7). Instead, we use Median Absolute Deviation (MAD) which is calculated with: $MAD = \text{median}(|Z_i - \tilde{Z}|)$, where $Z = 500$ predictions for a single set of inputs (x), Z_i is an individual prediction, and \tilde{Z} is $\text{median}(Z)$. A smaller MAD indicates lower variance and therefore a greater level of confidence in the

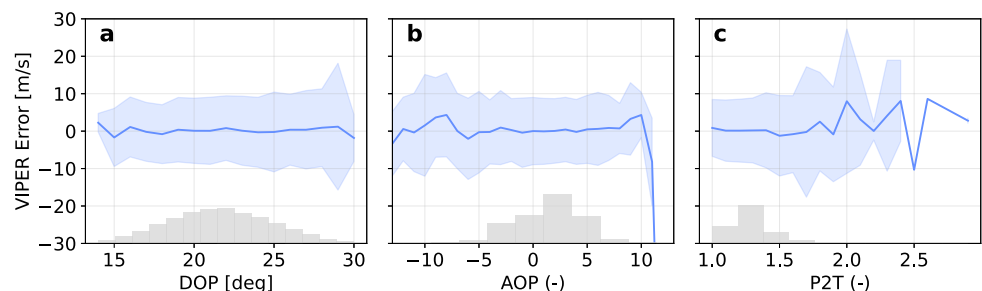


Figure 6. VIPER errors across the engineered EIA features. 0 m/s is a perfect score. The gray histograms represent the data availability.

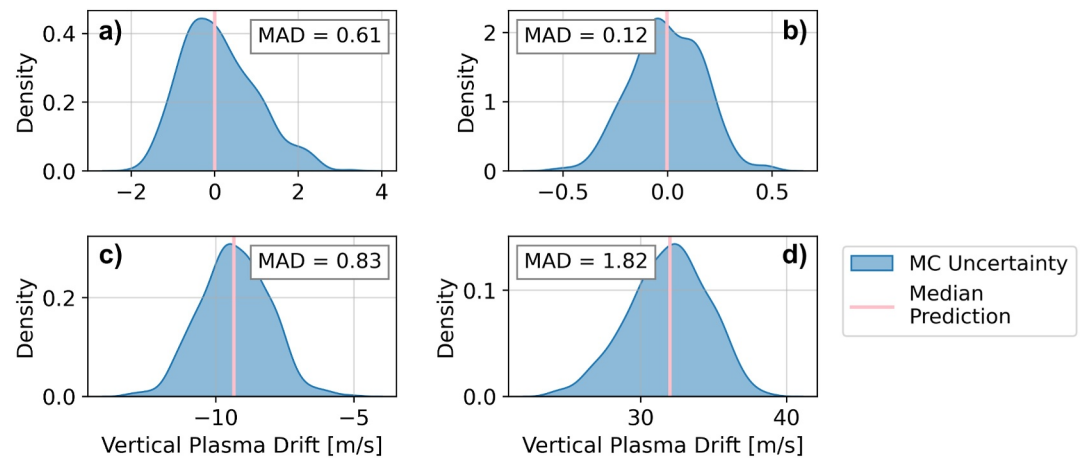


Figure 7. Four examples of uncertainty quantification via the Monte Carlo dropout method. The probability distribution is non-Gaussian and so median absolute deviation [m/s] is used to quantify the prediction distribution.

prediction. As seen, the uncertainty varies among predictions, even if the predicted value of v_z is the same: for example, 0 m/s (Figures 7a and 7b). For these two predictions the MAD varies from 0.12 to 0.61 m/s. As the magnitude of the plasma drift increases, so too does the MAD, with a prediction of -9.5 m/s having a MAD of 0.83 m/s (Figure 7c), and 32 m/s with MAD = 1.82 m/s (Figure 7d). This analysis shows that uncertainty is both non-Gaussian and non-uniform, even amongst identical predictions of drift (i.e., $v_z = 0$ m/s).

Comparing errors to uncertainty: MAE (Equation 8) shows how far off predictions are on average, while MC dropout shows how confident the model is about a *specific* prediction of v_z . To calculate the total error on predictions we simply combine the two: Error = MAE + MAD.

5.3. Preliminary Daily Prediction

The following example shows an initial investigation into VIPER's ability to make daily predictions of vertical plasma drift between -5° and 5° Mlat. In this example, the selected date is excluded from the training process and VIPER has not seen this datum before making predictions. Figure 8 shows VIPER predictions of vertical drift for four longitude sectors on 2014-03-16, a near equinox day with low geomagnetic activity. The drift is upward during the daytime, downward at night, and the pre-reversal enhancement is captured around sunset (~ 18 MLT). These basic features align with the climatological pattern derived from averaging AE-E and ROCSAT-1 drift

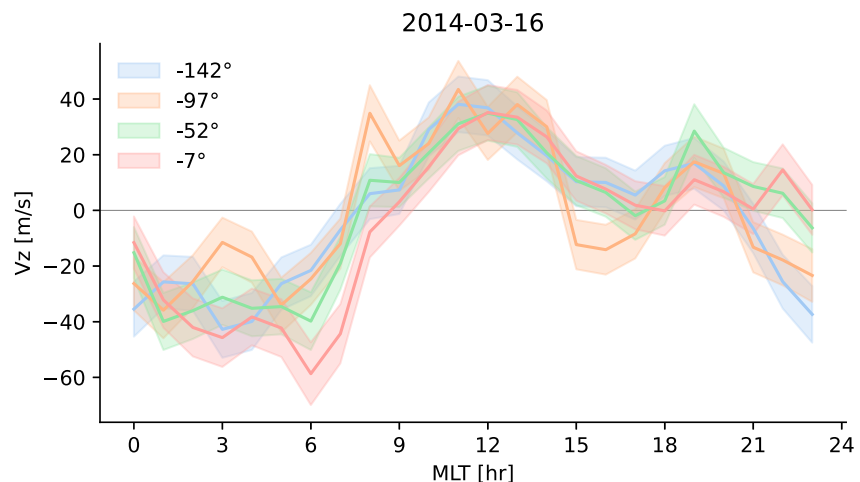


Figure 8. Daily predictions of vertical plasma drift as a function of magnetic local time and geographic longitude between -5° and 5° Mlat. Error bars are calculated with MAE + MAD.

observations during similar levels of solar activity (Fejer et al., 1995, 2008) and from the drift empirical model (Scherliess & Fejer, 1999). Across the longitudes we can see subtle differences in the drift predictions with respect to the climatological models, and this may be attributed to the daily nature of the drift. That said, VIPER might also be making noisier predictions.

VIPER is intended to reproduce vertical plasma drift by incorporating physical information embedded in 2D patterns of TEC maps. Although the preliminary results are promising, it is important to note that TEC coverage at low latitudes is poor in certain longitude sectors, particularly over oceans, as shown in Figure 1. The C/NOFS data also show large errors near the solar minimum during 2009–2010. These subsequently affect the model performance. The results indicate that further development is necessary to reduce noise and increase the accuracy, which can be pursued in the future by dealing with TEC data coverage and augmenting drift data for further training VIPER.

6. Discussion

VIPER has a MAE of 8.3 m/s, association of R : 0.89, and skill of PE: 0.78, all of which are considered good scores. The model performs well across a range of spatial-temporal and seasonal conditions and produces the best results when the availability of the data is highest. Monte Carlo techniques provide mathematically rigorous estimates of prediction uncertainty improving the utility of the model. VIPER showcases some promising preliminary results into daily (weather) predictions of v_z . This section will compare VIPER with the existing vertical drift and vertical $\mathbf{E} \times \mathbf{B}$ drift models. Additionally, it will discuss the Gaussian fitting procedure and provide preliminary insights into conceivable storm-time performance.

6.1. Comparing Models

Scherliess and Fejer (1999) developed an empirical model of vertical drift using the Atmospheric-Explorer E spacecraft data (1977–1979) and the Jicamarca ground station data (1968–1992). Their model focuses on daytime drifts and, like this study, also limits its scope to geomagnetically quieter conditions, $K_p < 3$. The Scherliess and Fejer (1999) model appears to be more of a climatological model, outputting predictions at seasonal time scales (e.g., May–August, November–February, and equinox), but finer resolutions might be achievable. The Scherliess and Fejer (1999) also includes vertical plasma data across 2.5 solar cycles, which is far greater than 0.5 cycle for this study.

Anderson et al. (2004) built a machine learning model to predict daytime vertical $\mathbf{E} \times \mathbf{B}$ drift between 10–16 LT, presenting an error of 2.9 m/s, although it is not known whether this is on the training or test set. VIPER has a test set MAE of 8.3 m/s, but can perform at all hours (0–23 LT). Further, Anderson et al. (2004) are predicting vertical $\mathbf{E} \times \mathbf{B}$ drift with geomagnetic perturbation in horizontal direction (ΔH), whereas VIPER predicts *all* vertical drift, including the equatorial vertical $\mathbf{E} \times \mathbf{B}$ drift, with TEC. The use of TEC data for daily predictions is appealing since the data can be readily obtained from several sources and has a low cost of operation.

More recently, Shidler and Rodrigues (2020) also used an ML approach to predict localized vertical drifts using the Jicamarca observatory data, comparing their results to the Scherliess and Fejer (1999) model. On the test set, VIPER has an R^2 of 0.8 and their random forest model has an R^2 of 0.71. Their model does not include MLT or a geomagnetic index as an input, which we have shown to have a strong influence on vertical plasma drift. The Shidler and Rodrigues (2020) model also covers a full 24 hr period, with higher data availability post-midnight compared to this study as they are not constrained by the minimum O^+ density requirement which exists on the C/NOFS IVM. Both VIPER and the Shidler and Rodrigues (2020) model include altitude, which has been shown to influence vertical drift in a linear manner (Pingree & Fejer, 1987), that is, faster drifts occur at higher altitudes. This might explain why altitude is marked as the least important feature in the Shidler and Rodrigues (2020), model, but its removal from the VIPER input space resulted in a non-trivial drop in performance. We have not investigated the reasons for this further at this stage.

Finally, all non-coupled first-principle ionospheric models require vertical $\mathbf{E} \times \mathbf{B}$ drift velocity as an input to predict the EIA (e.g., Bailey et al., 1997). Subsequently, the VIPER model could be used as a physics-surrogate to provide the necessary vertical $\mathbf{E} \times \mathbf{B}$ drift inputs (around 0° Mlat) for frameworks such as physics-based first-principle ionospheric models.

6.2. Gaussian Fits

Figure 2 shows the Gaussian fitting routine in action. A Gaussian method was chosen because of the likeness of the EIA in two-dimensions to a pair of normal distributions. This is shown in Figure 2 and is justified by the low χ^2_r scores in Figures 2c and 2d. From a physics perspective, this process is driven by the fountain effect. Whilst a Gaussian distribution is deterministic, the natural phenomena it describes are often associated with randomness. For example, the central limit theorem states that for a large enough sample of independent and random variables, their final approximate distribution will be Gaussian. Therefore, it would be advantageous to explore whether other functional forms are more appropriate.

6.3. Increasing Geomagnetic Activity

At present, VIPER has been capped at predicting vertical plasma drift during quiet and unsettled times only ($K_p \leq 3$). The complexity of a prediction increases with geomagnetic activity, which, when lacking sufficient storm-time data, could result in an unrealistic or inaccurate model. Therefore, we focused on capturing $K_p \leq 3$ conditions first, with a view to adding storm-time effects later. This means that VIPER is largely predicting v_z based on the effects of equatorial E and F region dynamics (Fejer et al., 1995; Immel et al., 2021). Under active geomagnetic conditions, prompt penetration electric fields and the disturbance dynamo can modify vertical drift and thus the EIA (e.g., Pi et al., 2003). Existing studies have shown that ML models exhibit unusual behavior when predicting events at, or beyond, the boundary of their training distribution. Smith et al. (2020) looked at four different models and showed the results of predictions that were out of distribution. Each exhibited very different behavior, presenting different predictions despite being more similar within the training distribution. This provides a cautionary tale for interpreting ML results when data is sparse. To conclude, VIPER could be expanded to include storm-time data and increased levels of geomagnetic activity, but more storm-time data is required. The inclusion of drift data from AE-E (e.g., Scherliess & Fejer, 1999), ICON, the planned Global Dynamics Constellation (Akbari et al., 2024), or localized ground based observations (e.g., Shidler & Rodrigues, 2020) could help improve model performance. Alternatively, these data sets could be used as further validation of the model performance in addition to the test and validation sets.

7. Conclusions

This study introduced a novel neural network model called VIPER which uses TEC data to predict vertical plasma drift in the low latitude and equatorial ionosphere. The main findings from this study are outlined below:

- The 2D distribution of the EIA at fixed local times resembles a Gaussian distribution. By fitting this, we can extract the width, magnitude, and peak of the EIA, before feeding it into the model. These quantities are linked to v_z , which helps to make VIPER physics-informed.
- A novel process has been developed whereby the TEC data passes through a series of checks with additional features added along the way (see Figure A1 of Appendix A). This includes adding new physical products or parameters like P2T, DOP and AOP.
- VIPER has a MAE of 8.3 m/s, R of 0.89, and PE of 0.78, all of which are considered respectable scores. VIPER predicts low-latitude vertical plasma drift across a range of spatial-temporal, seasonal and geomagnetic conditions, with no obvious bias for over- or under-estimating drift magnitudes.
- The findings indicate that the TEC GIMs include physical information useful to predictions at all times. This could pave the way for future studies ionospheric dynamics with TEC data, which can be readily obtained from global and regional GNSS networks.
- VIPER can reproduce vertical plasma drift at 24 hr resolution, which is necessary to capture the day-to-day (weather) variability of the ionosphere. However, the poor coverage of TEC data in certain longitude sectors and the large uncertainties in C/NOFS data during years near the solar minimum subsequently affect the model performance. Further development is necessary to reduce noise and increase the daily prediction accuracy, which can be pursued in the future by dealing with TEC data coverage and augmenting drift data for training VIPER.
- Uncertainty quantification reveals that the prediction itself can be interpreted as a probability distribution. The distributions are non-Gaussian, so the median and median absolute deviation are used to interpret the spread. They also reveal that identical predictions of v_z can have different error estimates and so bespoke MC error calculations are required each time.

- VIPER could be expanded to include geomagnetic storms, but there is much less data for these conditions and the effects on the overall model performance are not yet fully understood.

As summarized in the flowchart in Figure A1, the procedure of identifying and selecting key features and applying ML techniques is very promising. With ingestion of a constantly increasing database of observations from TEC and new satellites, VIPER can become a valuable ML tool for predicting daily vertical plasma drift, which modifies electron densities and consequently the integrity of satellite navigation and communications, amongst other impacts.

Appendix A

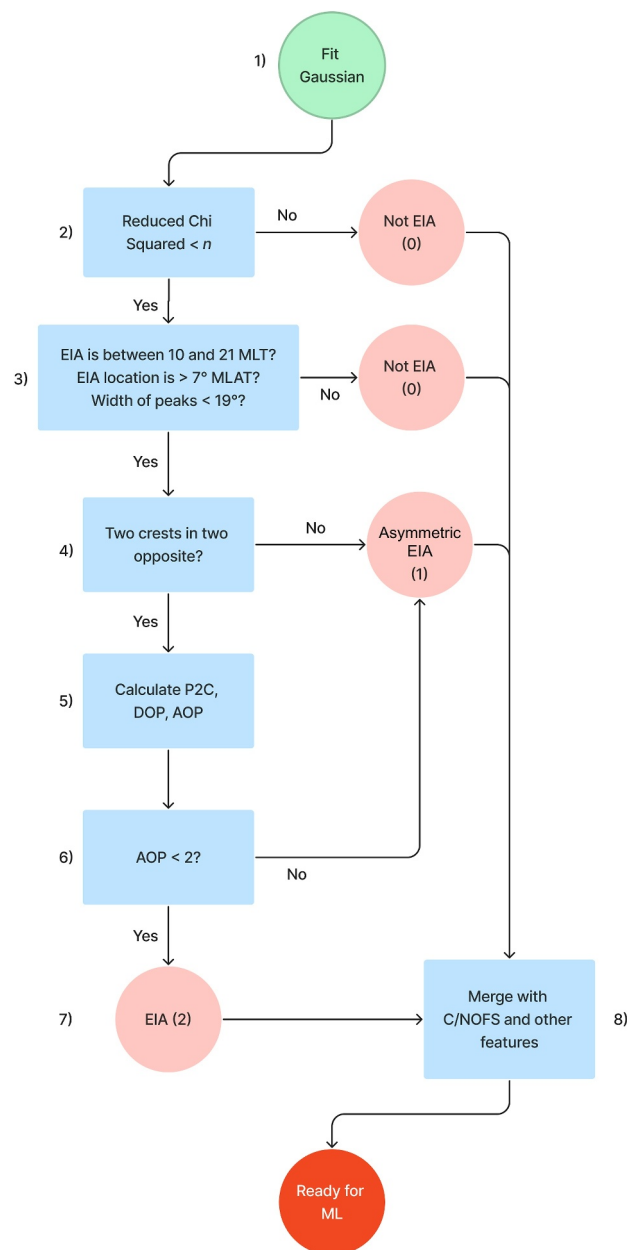


Figure A1. Cleaning and fitting the TEC data in preparation for VIPER training. Data are categorized into either no EIA (0), single peak (1), or double peak (2). This is then merged with C/NOFS and fed into the machine learning models. The main purpose of this process is to add more physical meaning to the input space and to aid interpretation.

Data Availability Statement

The Jet Propulsion Laboratory Global Ionospheric Maps (GIMs) are freely available via: https://sideshow.jpl.nasa.gov/pub/iono_daily/gim_for_research/jpld/. The Communication/Navigation Operations Forecasting System and OMNI data is freely available at: <https://hapi-server.org/servers/#server=CDAWeb>. The major Python packages used include: PyTorch, NumPy, Matplotlib, scikit-learn, and pandas. The VIPER model (model, scaler, and weights) is available at: <https://github.com/reddy-sachin/VIPER-TEC> as well as a .ipynb script to reproduce Figure 8.

Acknowledgments

This research was carried out at University College London with Science & Technology Facilities Council Grant ST/R505171/1 and at the Jet Propulsion Laboratory, California Institute of Technology, under a contract with the National Aeronautics and Space Administration (80NM0018D0004). The authors are thankful to the Ionospheric and Atmospheric Remote Sensing group of the Jet Propulsion Laboratory for making GIM products available to the public for research.

References

- Akbari, H., Rowland, D., Coleman, A., Buynovskiy, A., & Thayer, J. (2024). Gradient calculation techniques for multi-point ionosphere/thermosphere measurements from GDC. *Frontiers in Astronomy and Space Sciences*, 11, 1231840. <https://doi.org/10.3389/fspas.2024.1231840>
- Anderson, D., Anghel, A., Chau, J., & Veliz, O. (2004). Daytime vertical $\mathbf{E} \times \mathbf{B}$ drift velocities inferred from ground-based magnetometer observations at low latitudes. *Space Weather*, 2(11), 2004SW000095. <https://doi.org/10.1029/2004SW000095>
- Appleton, E. (1946). Two anomalies in the ionosphere. *Nature*, 157(3995), 691. <https://doi.org/10.1038/157691a0>
- Bailey, G. J., Balan, N., & Su, Y. Z. (1997). The Sheffield University plasmasphere ionosphere model—A review. *Journal of Atmospheric and Solar-Terrestrial Physics*, 59(13), 1541–1552. [https://doi.org/10.1016/S1364-6826\(96\)00155-1](https://doi.org/10.1016/S1364-6826(96)00155-1)
- Balan, N., Liu, L. B., & Le, H. J. (2018). A brief review of equatorial ionization anomaly and ionospheric irregularities. *Earth and Planetary Physics*, 2(4), 257–275. <https://doi.org/10.26464/epp2018025>
- Balan, N., Rajesh, P. K., Sripathi, S., Tulasiram, S., Liu, J. Y., & Bailey, G. J. (2013). Modeling and observations of the north–south ionospheric asymmetry at low latitudes at long deep solar minimum. *Advances in Space Research*, 52(3), 375–382. <https://doi.org/10.1016/j.asr.2013.04.003>
- Chai, T., & Draxler, R. R. (2014). Root mean square error (RMSE) or mean absolute error (MAE)?—Arguments against avoiding RMSE in the literature. *Geoscientific Model Development*, 7(3), 1247–1250. <https://doi.org/10.5194/gmd-7-1247-2014>
- De La Beaujardière, O. (2004). C/NOFS: A mission to forecast scintillations. *Journal of Atmospheric and Solar-Terrestrial Physics*, 66(17), 1573–1591. <https://doi.org/10.1016/j.jastp.2004.07.030>
- Emmert, J. T., Richmond, A. D., & Drob, D. P. (2010). A computationally compact representation of Magnetic-Apex and Quasi-Dipole coordinates with smooth base vectors. *Journal of Geophysical Research*, 115(A8), 2010JA015326. <https://doi.org/10.1029/2010JA015326>
- Fejer, B. G., de Paula, E. R., Heelis, R. A., & Hanson, W. B. (1995). Global equatorial ionospheric vertical plasma drifts measured by the AE-E satellite. *Journal of Geophysical Research*, 100(A4), 5769–5776. <https://doi.org/10.1029/94ja03240>
- Fejer, B. G., Jensen, J. W., & Su, S. Y. (2008). Quiet time equatorial F region vertical plasma drift model derived from ROCSAT-1 observations. *Journal of Geophysical Research*, 113(5). <https://doi.org/10.1029/2007JA012801>
- Gal, Y., & Ghahramani, Z. (2016). Dropout as a Bayesian approximation: Representing model uncertainty. In *Deep learning* (pp. 1050–1059).
- Hanson, W. B., & Moffett, R. J. (1966). Ionization transport effects in the equatorial F region. *Journal of Geophysical Research*, 71(23), 5559–5572. <https://doi.org/10.1029/JZ071i023p05559>
- Huang, H., Lu, X., Liu, L., Wang, W., & Li, Q. (2018). Transition of interhemispheric asymmetry of equatorial ionization anomaly during solstices. *Journal of Geophysical Research: Space Physics*, 123(12), 2018JA026055. <https://doi.org/10.1029/2018JA026055>
- Iijima, B. A., Harris, I. L., Ho, C. M., Lindqwister, U. J., Mannucci, A. J., Pi, X., et al. (1999). Automated daily process for global ionospheric total electron content maps and satellite ocean altimeter ionospheric calibration based on Global Positioning System data. *Journal of Atmospheric and Solar-Terrestrial Physics*, 61(16), 1205–1218. [https://doi.org/10.1016/S1364-6826\(99\)00067-X](https://doi.org/10.1016/S1364-6826(99)00067-X)
- Immel, T. J., Harding, B. J., Heelis, R. A., Maute, A., Forbes, J. M., England, S. L., et al. (2021). Regulation of ionospheric plasma velocities by thermospheric winds. *Nature Geoscience*, 14(12), 893–898. <https://doi.org/10.1038/s41561-021-00848-4>
- Kil, H., Oh, S., Paxton, L. J., & Fang, T. (2009). High-resolution vertical $\mathbf{E} \times \mathbf{B}$ drift model derived from ROCSAT-1 data. *Journal of Geophysical Research*, 114(A10), 2009JA014324. <https://doi.org/10.1029/2009JA014324>
- Liemohn, M. W., Shane, A. D., Azari, A. R., Petersen, A. K., Swiger, B. M., & Mukhopadhyay, A. (2021). RMSE is not enough: Guidelines to robust data-model comparisons for magnetospheric physics. *Journal of Atmospheric and Solar-Terrestrial Physics*, 218, 105624. <https://doi.org/10.1016/j.jastp.2021.105624>
- Mannucci, A. J., Wilson, B. D., Yuan, D. N., Ho, C. H., Lindqwister, U. J., & Runge, T. F. (1998). A global mapping technique for GPS-derived ionospheric total electron content measurements. *Radio Science*, 33(3), 565–582. <https://doi.org/10.1029/97RS02707>
- Martyn, D. (1955). Theory of height and ionization density changes at the maximum of a Chapman-like region, taking account of ion production, decay, diffusion and tidal drift. *Physics of the Ionosphere*, 254.
- van der Meeren, C., Laundal, K., Burrell, A., Starr, G., Reimer, A., & Morschhauser, A. (2021). ApexPy (Version 1.1.0) [Computer software]. *Zenodo*. <https://doi.org/10.5281/zenodo.4585641>
- Mitra, S. (1946). Geomagnetic control of region F2 of the ionosphere. *Nature*, 158(4019), 668–669. <https://doi.org/10.1038/158668a0>
- More, J. J. (1978). The Levenberg-Marquardt algorithm: Implementation and theory. In G. A. Watson (Ed.), *Numerical analysis* (Vol. 630, pp. 105–116). Springer Berlin Heidelberg. <https://doi.org/10.1007/BFb0067700>
- Murphy, A. H. (1988). Skill scores based on the mean square error and their relationships to the correlation coefficient. *Monthly Weather Review*, 116(12), 2417–2424. [https://doi.org/10.1175/1520-0493\(1988\)116<2417:SSBOTM>2.0.CO;2](https://doi.org/10.1175/1520-0493(1988)116<2417:SSBOTM>2.0.CO;2)
- Pi, X., Mannucci, A. J., Iijima, B. A., Wilson, B. D., Komjathy, A., Runge, T. F., & Akopian, V. (2009). Assimilative modeling of ionospheric disturbances with FORMOSAT-3/COSMIC and ground-based GPS measurements. *Terrestrial, Atmospheric and Oceanic Sciences*, 20(1), 273. [https://doi.org/10.3319/TAO.2008.01.04.01\(F3C\)](https://doi.org/10.3319/TAO.2008.01.04.01(F3C))
- Pi, X., Wang, C., Hajj, G. A., Rosen, G., Wilson, B. D., & Bailey, G. J. (2003). Estimation of $\mathbf{E} \times \mathbf{B}$ drift using a global assimilative ionospheric model: An observation system simulation experiment. *Journal of Geophysical Research*, 108(A2), 2001JA009235. <https://doi.org/10.1029/2001JA009235>
- Pingree, J. E., & Fejer, B. G. (1987). On the height variation of the equatorial F region vertical plasma drifts. *Journal of Geophysical Research*, 92(A5), 4763–4766. <https://doi.org/10.1029/JA092iA05p04763>
- Popescu, M.-C., Balas, V. E., Perescu-Popescu, L., & Mastrokakis, N. (2009). Multilayer perceptron and neural networks. 8(7).

- Richmond, A. D. (1995). Ionospheric electrodynamics using magnetic apex coordinates. *Journal of Geomagnetism and Geoelectricity*, 47(2), 191–212. <https://doi.org/10.5636/jgg.47.191>
- Scherliess, L., & Fejer, B. G. (1999). Radar and satellite global equatorial F region vertical drift model. *Journal of Geophysical Research*, 104(A4), 6829–6842. <https://doi.org/10.1029/1999ja900025>
- Shidler, S. A., & Rodrigues, F. S. (2020). Modeling equatorial ionospheric vertical plasma drifts using machine learning. *Earth Planets and Space*, 72(1), 102. <https://doi.org/10.1186/s40623-020-01227-w>
- Smith, A. W., Rae, I. J., Forsyth, C., Oliveira, D. M., Freeman, M. P., & Jackson, D. R. (2020). Probabilistic forecasts of storm sudden commencements from interplanetary shocks using machine learning. *Space Weather*, 18(11), e2020SW002603. <https://doi.org/10.1029/2020SW002603>
- Srivastava, N., Hinton, G., Krizhevsky, A., Sutskever, I., & Salakhutdinov, R. (2014). Dropout: A simple way to prevent neural networks from overfitting. *Journal of Machine Learning Research*, 15, 1929–1958.